Light Scattering Study of Rigid, Rodlike Organometallic Block Copolymer Micelles in Dilute Solution

Gérald Guérin, Jose Raez, Ian Manners,* and Mitchell A. Winnik*

Department of Chemistry, University of Toronto, 80 St. George Street, Toronto, Ontario M5S 3H6, Canada

Received January 14, 2004; Revised Manuscript Received July 12, 2005

ABSTRACT: The block copolymer poly(ferrocenyldimethylsilane-*b*-dimethylsiloxane) (PFS_{40}-*b*-$PDMS_{480}$, where the subscripts refer to the mean degree of polymerization) self-assembles in *n*-decane at 25 °C to form long rodlike micelles (Raez et al. *J. Am. Chem. Soc*. **2002**, *124*, 10381). Here, we describe a combination of static (SLS) and dynamic (DLS) light scattering measurements on solutions of the micelles in *n*-decane. By SLS, we find that the micelles are thin, rigid, rodlike structures with a mean length of ∼960 nm in the limit of zero concentration and a length that increases with concentration. Through a combination of SLS and DLS measurements, we find that that the cross-sectional hydrodynamic diameter of the micelle is 18 nm. These self-assembled structures also appear to have a narrow distribution of lengths (with $M_w/M_n \approx 1.1$). These structures are much smaller than those observed on transmission electron microscopy (TEM) grids obtained from solutions of these self-assembled structures.

Introduction

Diblock copolymers consisting of a poly(ferrocenyldimethylsilane) strand connected to a poly(dimethylsiloxane) strand (PFS-*b*-PDMS) self-assemble to form interesting and unusual structures in alkane solvents.[1,2] For example, PFS_{50}-*b*-$PDMS_{300}$ (the subscripts refer to the mean degree of polymerization) forms dense cylindrical micelles in *n*-hexane.[2] Simple alkanes are modest to poor solvents for PDMS but nonsolvents for PFS. The insolubility of the PFS should drive the self-assembly process, but the formation of cylinders is surprising. Most asymmetric diblock copolymers associate in solvents selective for the longer block to form spherical micelles.[3] A common feature of these micelles is that the insoluble block is an amorphous polymer.[4] PFS is a semicrystalline polymer.[5] Wide-angle X-ray scattering measurements on films formed from solutions of the cylindrical micelles exhibit peaks consistent with the presence of crystalline domains of PFS in the micelle.[5]

Block copolymers with a crystallizable block in a selective solvent normally form aggregates in the form of raftlike structures, with the soluble chains protruding from the two surfaces.[6] This structure is consistent with the idea that polymers crystallize best in lamellar domains. For example, in the Vilgis and Halperin[7] model, this block forms crystals through adjacent folds within the core, and a sharp interface divides the crystalline core from the solvent-swollen corona. The overall shape of the self-assembled structure depends on the interplay between the interfacial energy between the crystalline block and the solvent and stretching within the amorphous block due to overlap of adjacent coils. Cao et al.[8] have reported that polyisoprene block copolymers of PFS (PFS-*b*-PI) form these kinds of planar structures in hexane when the soluble PI block is shorter than the PFS block, but when the PI block is longer, cylindrical structures were observed by transmission electron microscopy (TEM).

* To whom correspondence should be addressed. E-mail: imanners@chem.utoronto.ca (I.M.); mwinnik@chem.utoronto.ca (M.A.W.).

The behavior of PFS-*b*-PDMS is even more interesting. In the example mentioned above, the ratio of the PFS length to the PDMS length was 1:6. When polymers were synthesized with longer block length ratios (1:12 and 1:18), the structures formed in *n*-hexane appeared in the TEM images to be hollow nanotubes[9,10] with a core diameter of ∼20 nm and a wall thickness of ∼7 nm.[9] Similar structures formed in *n*-decane. The 1:12 polymer PFS_{40}-*b*-$PDMS_{480}$ is not soluble in decane at room temperature, but samples dissolved at 60 °C, cooled to room temperature, allowed to age for a day, and then examined by TEM showed that the polymer formed long nanotubes with lengths on the order of tens of micrometers. We have recently established that these structures form reversibly.[11] When a solution of this polymer was heated to 50 °C and examined by TEM, we observed relatively short dense rods. When the solution was cooled back to 25 °C, the system rearranged over the course of 24 h back to the same nanotube-like structures observed previously. This process could be repeated several times.

In this paper, we describe preliminary results of static (SLS) and dynamic (DLS) light scattering experiments on solutions of these micelles in decane at 25 °C. The SLS and DLS data indicate that the structures present in *n*-decane solution are much smaller than those seen in the TEM images. They are thin rodlike structures, ∼960 nm long, consisting of ∼580 polymer molecules per micelle in the limit of zero concentration. Moreover, their width appears to increase with concentration, suggesting that a second level of hierarchical self-assembly occurs.

Experimental Section

Materials, Synthesis, and Characterization. *n*-Decane (99+% pure), toluene, tetrahydrofuran (THF), and acetone (all reagent grade) were purchased from Aldrich and used without further purification. The copolymer PFS_{40}-*b*-$PDMS_{480}$ is the same sample described in our previous publications, and full details are provided elsewhere.[9,12] It was synthesized by two-stage anionic polymerization, beginning with *n*-butyllithium initiated polymerization of the strained silicon-bridged [1]-ferrocenophane and the subsequent addition of hexamethyl-

10.1021/ma0498870 CCC: $30.25
Published on Web 08/13/2005

trisiloxane (D_3). The reaction was terminated with chlorotrimethylsilane. The copolymer sample was purified in a size exclusion column with tetrahydrofuran (THF) as the solvent. From gel permeation chromatography (GPC)[13] and ^{1}H NMR experiments, we determined that M_n(PFS) = 9700 g/mol, M_n-(diblock) = 45 300, and M_w/M_n = 1.01.[9]

Sample Preparation for Transmission Electron Microscopy. Micelle solutions in *n*-decane (bp 174 °C) were prepared by adding 10 mL of solvent to 10 mg of block copolymer in a flask, which was then placed in a preheated oven or oil bath at 60 °C for 30 min. *n*-Decane does not dissolve the block copolymer at room temperature. Then, the mixture was allowed to cool to room temperature. TEM samples were prepared at this temperature (23 °C) by placing a 7 μL sample of the micelle solution onto a precoated copper grid which was placed on a filter paper or by immersing a precoated copper grid into the solution. Excess fluid was then removed with a clean piece of filter paper. TEM images were obtained with a Hitachi model 600 electron microscope working at 75 kV. Before every TEM session, the electron beam was aligned to minimize optical artifacts. Sizes of objects in the TEM micrographs were measured using Adobe Photoshop 4.0.

Sample Preparation for Light Scattering Measurements. Disposable 10 mm × 75 mm glass cells for light scattering were purchased from Fisher Scientific Chemicals. These were cleaned in an acetone still for 15 min. The cells were then removed from the still, and the open end was immediately tightly wrapped with Al foil. Sealed cells were placed in an oven at 120 °C for 1 h to evaporate any residual acetone trapped in the cell.

Micelle solutions of PFS_{40}-*b*-$PDMS_{480}$ in *n*-decane for light scattering studies were prepared by two different techniques. The first consisted of slowly injecting, through 0.2 μm pore filters, 0.1 mL aliquots of a PFS_{40}-*b*-$PDMS_{480}$ solution in tetrahydrofuran (THF, 10 mg/mL) into preweighed sealed cells by perforating the Al foil of each cell with the syringe needle. The cells were again covered with Al foil and placed in an oven set at 55 °C for 4 h. At this point, the THF had evaporated from the cells. The cells were weighed again in order to obtain the net weight of the polymer in the tube. Filtered *n*-decane was then added to the cells. After the cells were capped, Teflon tape was wrapped around the caps to avoid any solvent evaporation or infiltration of dust. On the basis of the weight of the added *n*-decane, the final concentration was determined. The samples were then placed in the preheated vat (60.0 °C) of the light scattering equipment to dissolve the polymer in *n*-decane. The samples were then cooled to 25 °C.

The second technique consisted of heating a PFS_{40}-*b*-$PDMS_{480}$ sample in *n*-decane at 60 °C for 30 min in a closed vial. The solution was allowed to cool to room temperature and then injected into the Al-foil-sealed cells through a 0.5 μm pore size filter. Finally, Teflon tape was wrapped around the caps of the cells. The solutions were allowed to equilibrate for 1 day at ambient temperature prior to carrying out our light scattering experiments. As a comment on this sample preparation technique, we note that the micelle formation rate is slow and that the structures present in solution at this time are still small enough to pass through the filter.

Light Scattering Equipment. Differential refractive indices (dn/dc) were measured using a BI-DNDCW refractometer (Brookhaven Instruments Co.). The refractometer uses a red laser (λ_0 = 620 nm) as a light source. Before any measurements were taken, the instrument was calibrated with solutions of poly(methyl methacrylate) (M_p = 400 000 g/mol, M_w/M_n = <1.14, Polymer Laboratories Ltd.) in THF, for which dn/dc = 0.0877 mL/g at 30 °C.

Static (SLS) and dynamic light scattering (DLS) measurements were performed using a wide-angle light scattering photometer from ALV. The light source was a JDS Uniphase He−Ne laser (λ_0 = 632.8 nm, 35 mW) emitting vertically polarized light. The cells were placed into the ALV/DLS/SLS-5000 Compact Goniometer System and sat in a vat of thermostated *cis*-decahydronaphthalene, which matched the index of refraction of the glass cells. The angular range of the goniometer is 12−155°. The scattered light was detected by a Dual ALV−High Q.E. APD avalanche photodiode module. This detector was interfaced to the ALV-5000/EPP multiple tau digital correlator with 288 exponentially spaced channels that measured the correlation function in real time. The vat was connected to an F25-HE Jubalo heating circulator. All measurements were carried out at 25.0 ± 0.05 °C. For SLS experiments, two angular ranges were investigated. The first range consisted of scattering angles between 27 and 36° (at 3° intervals), while the second range consisted of angles between 40 and 150° (at 5° intervals). DLS measurements were performed at angles between 30 and 150° (with 10° intervals). Filtered toluene was used as the standard in the SLS measurements.

For polarized (VV) DLS, a polarizer was placed in front of the photodiode, and its orientation was adjusted to give the maximum intensity for a solution of poly(isoprene-*b*-methyl methacrylate) spherical micelles in acetonitrile.[14] This orientation ensured that vertically polarized light entered the detector. The value for the viscosity of *n*-decane at 25 °C was obtained from the literature.[15] Autocorrelation functions were analyzed using the ALV-Correlator Software v 3.0. The different types of data analysis will be described in the following section.

Theory and Data Analysis. Dynamic Light Scattering. The measured intensity−intensity time-correlation function, $g^{(2)}(t_c)$, where t_c is the delay time, was related to the normalized electric field correlation function, $g^{(1)}(t_c)$, representative of the motion of the particles, by the Siegert relation.[16] As t_c increases, $g^{(1)}(t_c)$ will decay. The decay of $g^{(1)}(t_c)$ with increasing delay time carries information about the diffusion of the particles in solution. For monodisperse spherical particles undergoing Brownian motion, the decay curve can be described by a single-exponential term, $g^{(1)}(t_c) = \exp(-\Gamma t_c)$, where the relaxation rate, Γ, is related to the mutual diffusion coefficient, D_m, of the diffusing species as $\Gamma = q^2 D_m$. Thus, a plot of Γ versus q^2 should be linear with slope D_m and pass through the origin.

For rigid extended systems, one expects a more complex decay due to rotation−diffusion coupling, and for polydisperse systems, $g^{(1)}(t_c)$ is characterized by a sum of exponential components in terms of the delay time, t_c, reflecting the distribution of relaxation rates. Here, $g^{(1)}(t_c)$ can be related to the relaxation rate distribution, $G(\Gamma)$, through the following expression:

$$g^{(1)}(t_c) = \int_0^\infty G(\Gamma) \exp(-\Gamma t_c)\, d\Gamma \qquad (1)$$

Laplace inversion of eq 1 gives $G(\Gamma)$. In this study, the inversion was calculated with the program CONTIN[17] included in the ALV software. We analyzed the results with a smoothing parameter of 0.5.

We also analyzed our data in terms of a cumulant expansion to third order (3-CUM) of the logarithm of $g^{(1)}(t_c)$.[18]

$$\ln g^{(1)}(t_c) = -\Gamma_1 t_c + \left(\frac{\mu_2}{2!}\right) t_c^{\,2} - \left(\frac{\mu_3}{3!}\right) t_c^{\,3} + \ldots \qquad (2)$$

where Γ_1 is the first cumulant and μ_2 and μ_3 are the second and third cumulants, respectively. The "true" diffusion constant, D_0, can be obtained from Γ_1 by extrapolation to zero concentration and zero scattering angle. For spherical particles, the hydrodynamic radius, R_h, can be calculated from D_0 by means of the Stokes−Einstein equation

$$R_h = \frac{k_B T}{6\pi\eta_0 D_0} \qquad (3)$$

where k_B is the Boltzmann constant, T is the temperature, and η_0 is the solvent viscosity. For experiments carried out at finite concentration and scattering angle, introducing D_m in place of D_0 in eq 3 yields an apparent hydrodynamic radius, $R_{h,app}$.

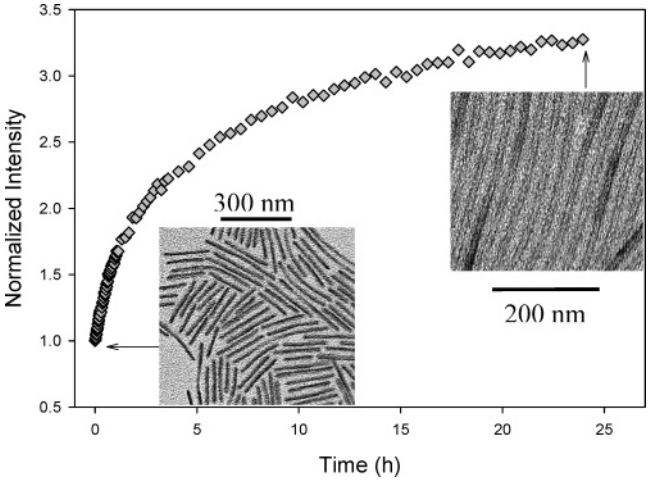

Figure 1. Evolution of the normalized light scattering intensity of a 0.8 mg/mL solution of PFS_{40}-*b*-$PDMS_{480}$ equilibrated at 50 °C in decane and then immersed into the vat of the light scattering apparatus at 25 °C. The TEM micrographs of the same sample taken at the beginning and at the end of the experiment are shown in the inset.

Results and Discussion

We are interested in the self-assembly process of PFS_{40}-*b*-$PDMS_{480}$ in *n*-decane at 25 °C. This polymer is very poorly soluble when added directly to decane at room temperature but dissolves when warmed. As described in ref 11, a droplet of this solution at 50 °C, when placed on a grid and examined by TEM, exhibits a relatively narrow distribution of rigid rods approximately 150 nm long with a width of ~20 nm. In these unstained images, the dominant contrast is from the iron-rich core, so that these dimensions pertain to the PFS core. Upon cooling to 23 or 25 °C, the system rearranges slowly to form a very different structure, which by TEM is seen to consist of apparently hollow nanotubes. These tubelike structures have an outer core width of ~20 nm and lengths of tens of micrometers. We are interested in learning how these tubelike structures form, and this paper describes our initial results in developing an understanding of what turns out to be a complex and subtle process.

To emphasize the slow rate of rearrangement of the system, we plot in Figure 1 the growth in total right-angle light scattering intensity of a solution of PFS_{40}-*b*-$PDMS_{480}$ equilibrated at 50 °C and then immersed into the vat of the light scattering apparatus at 25 °C. The growth in intensity is slow and monotonic. The initial and final morphologies seen by TEM are shown as insets to the plot. Over the 24 h course of the morphology evolution, the apparent hydrodynamic radius (at this concentration and scattering angle) increases from ~50 to 140 nm. While these are not true R_h values, it should be clear that the $R_{h,app}$ value at 25 °C is much smaller than that to be expected from a tubelike structure with a length greater than 10 μm.

To help clarify the nature of the species present in dilute solution, we carried out static and dynamic light scattering experiments for solutions of PFS_{40}-*b*-$PDMS_{480}$ in decane at 25 °C. As described in the Experimental Section, samples were prepared in two ways to ensure that sample filtration did not remove objects of interest from the scattering solution. In one approach, a filtered solution of the polymer in THF was introduced into the scattering cell. The solvent was removed, and a known amount of filtered decane was added. The solution was then heated to 60 °C, cooled to 25 °C, and allowed to age for 24 h. In the second method, a solution in decane prepared at 60 °C was cooled to room temperature and filtered directly into the light scattering cell through a 0.5 μm pore size filter. Both samples gave very similar light scattering signals.

For block copolymers, the total refractive index increment, $(dn/dc)_{net}$, can be expressed as the weighted sum of its components:[19,20]

$$\left(\frac{dn}{dc}\right)_{net} = f_F\left(\frac{dn}{dc}\right)_F + f_D\left(\frac{dn}{dc}\right)_D \quad (4)$$

where f_F and f_D are respectively the weight fractions of the F block and the D block and dn/dc is the refractive index increment of each block. From the measured values of the block copolymer micelles in decane ($(dn/dc)_{net} = 0.0465$ mL/g, $f_F = 0.214$) and that of PDMS ($(dn/dc)_D = -0.0104$ mL/g,[21] $f_D = 0.786$), we calculate $(dn/dc)_F$ to be 0.255 mL/g. We see that $(dn/dc)_F$ is much larger than $(dn/dc)_D$, and since $\Delta R \propto (dn/dc)^2$, the light scattering intensity will be due primarily to scattering by the PFS block. While information obtained from the angular dependence of the scattering intensity will pertain to that of the PFS block,[22] the molecular weight obtained from the light scattering conveys information about the entire self-assembled structure, because the dn/dc value accounts for the weight fraction of both blocks.[22,23]

Static Light Scattering (SLS) Experiments. In static light scattering (SLS), one obtains structural and dimensional information by measuring the angular dependence of the excess absolute time-averaged scattered intensity (the Rayleigh ratio, R_θ). For dilute solutions, R_θ is related to the sample concentration, c, the second viral coefficient, A_2, and the form factor, $P(q)$, through the following expression:[24]

$$\left(\frac{Kc}{R_\theta}\right) = \left[\frac{1}{M_w P(q)} + 2A_2 c\right] \quad (5)$$

where $K = 4\pi^2 n_{30}^2 (dn/dc)^2/(N_A \lambda^4)$ and N_A, λ, dn/dc, and n_D are Avogadro's number, the incident wavelength (632.8 nm), the refractive index increment, and the refractive index of the solvent, respectively.

SLS studies were performed at four different copolymer concentrations, c (0.33, 0.57, 0.75, and 0.85 mg/mL). Each solution was prepared at 60 °C and then was allowed to age for 24 h at 25 °C before data collection. Figure 2a shows the plot of Kc/R_θ as a function of q^2, at those four concentrations and the values extrapolated to zero concentration. The downward curvature of these different plots suggests that the scattering particles present in solution have a rodlike shape, which is emphasized by the Holtzer plateau observed when a Casassa−Holtzer representation (qR_θ/Kc vs q) is used (Figure 2b).

From the magnitude of the plateau (for $c = 0$), we can calculate the mass per unit length of the rods. We obtain a value of $M/L \approx 27\,000$ g/mol/nm, corresponding to an aggregation number of $n_L = 0.59$ molecules/nm. An unusual feature of this plot is that the plateau value increases with increasing concentration. This result indicates that the mass per unit length of the scattering particles increases with concentration, which is contrary to what one would expect for micelles formed by a closed association process. We will discuss this phenomenon at the end of the paper.

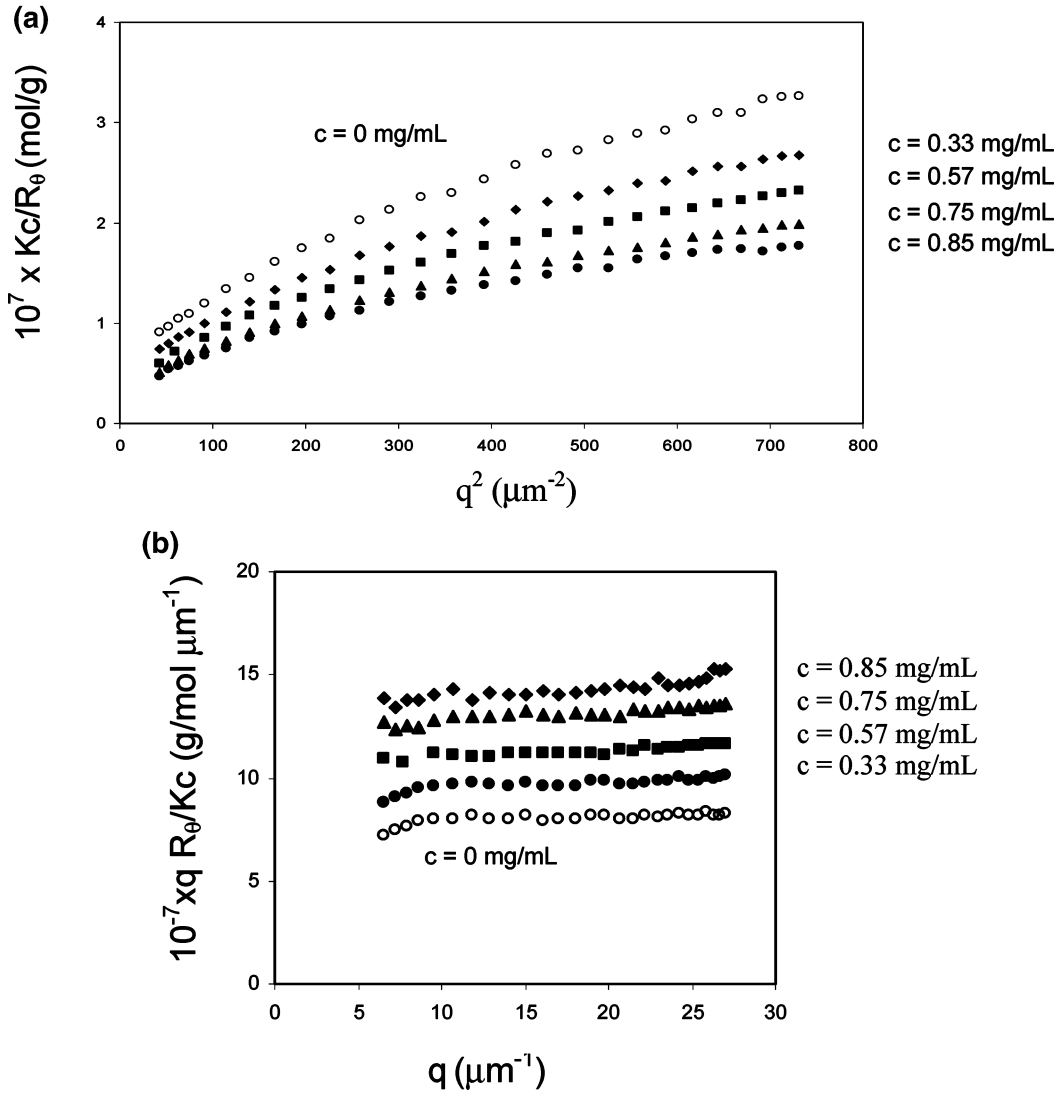

Figure 2. PFS_{40}-*b*-$PDMS_{480}$ assemblies in *n*-decane at 25 °C at four concentrations (0.33, 0.57, 0.75, and 0.85 mg/mL) and extrapolated at $c = 0$ (open symbols): (a) plots of Kc/R_θ as a function of q^2; (b) plots of qR_θ/Kc as a function of q. Each sample was dissolved in *n*-decane at 60 °C, cooled to room temperature, and then allowed to age for 24 h at 25 °C.

Another indication that the mass of the self-assembled objects present in solution increases with concentration can be seen in Figure 2a in the evolution of the apparent molecular weight of the micelle as a function of the $PFS_{40}-PDMS_{480}$ concentration. These values increase with the copolymer concentration, leading to an apparent negative second virial coefficient, A_2. Moreover, the increase of the downward curvature suggests that the length of the rodlike particle increases as a function of the concentration. The poor solvent quality of decane for PDMS may also contribute to the negative value of A_2. Inverse gas chromatography (IGC) measurements yield a Flory–Huggins χ-parameter for PDMS–decane of 0.64 at 25 °C.[25] While this value is appropriate for a dilute concentration of decane in PDMS and the χ-parameter is expected to vary with polymer–solvent composition, we infer that *n*-decane is a poor to marginal solvent for PDMS.

Determination of the Molecular Weight of the Micelles. The determination of the molecular weight of the micelles is complicated by the lack of data at low angles. A simple Zimm plot analysis of the $(Kc/R_\theta)_{c=0}$ curve cannot be performed in a straightforward way (as suggested by eq 5), since it would lead to an underestimated value of the molecular weight. As a consequence, we plotted $(Kc/R_\theta)_{c=0}$ as a function of q, since, according to Holtzer,[26] the Rayleigh ratio for rods reaches a linear asymptotic behavior at large values of qL, given by

$$\left(\frac{Kc}{R_\theta}\right)_{c=0} = \frac{1}{M_n}\left(\frac{2}{\pi^2} + \frac{1}{\pi}L_n q\right) \qquad (6)$$

where M_n and L_n are the number-averaged molecular weight and length of the rod, respectively. As can be seen in Figure 3, $(Kc/R_\theta)_{c=0}$ evolves linearly as a function of q, suggesting that it follows the asymptotic behavior described by eq 6. From the intercept and slope, respectively, we find that $M_n \approx (2.6 \pm 0.3) \times 10^7$ g/mol and $L_n \approx 960$ nm. In preparing this plot, we have disregarded the first two points at low q of Figure 3, and the error in M_n has been calculated by averaging several slopes obtained by taking into account, or not, the first remaining data at low q. The length of the micelles deduced from this method of data analysis confirms that the micelles can be considered to be long, thin rods. As we discuss in more detail below, we find a relatively narrow distribution of lengths. For example,

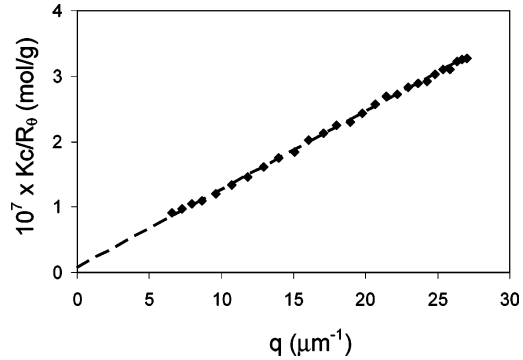

Figure 3. Plot of $(Kc/R_\theta)_{c=0}$ as a function of q (filled diamonds) extrapolated to $q = 0$ (dashed line).

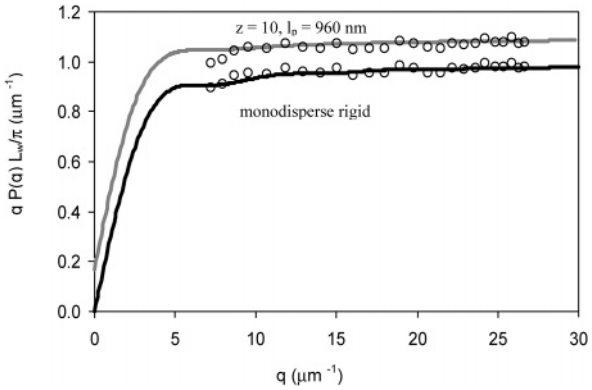

Figure 4. Plot of $qP(q)L_w/\pi$ as a function of q; comparison between the experimental data extrapolated to $c = 0$ (open circles) and the theoretical fit (solid line) of a population of monodisperse rigid rods (full black curve) and slightly flexible rods narrowdisperse in length, using $M_n = 2.6 \times 10^7$ g/mol, $L_n = 960$ nm, $l_p = 960$ nm, and $z = 10$ (corresponding to $M_w/M_n = 1.1$) as fitting parameters (see text for details). This second fit (curve and experimental data) has been arbitrarily shifted by 0.1 units for visual clarity.

from dynamic light scattering, we find that $\mu_2/\Gamma^2 = 0.12$ at 0.33 mg/mL. For rigid rods, the radius of gyration deduced from the expression $R_g = (L/12^{1/2})$ is 280 nm.

At large q, both the data and the theoretical fit are in excellent agreement, showing a slight discrepancy at low q which could be due to experimental error. An interesting consequence of this plot is that the aggregation number $n_L \approx 0.6$ molecules/nm obtained from the limiting slope corresponds to 580 molecules per micelle.

In Figure 4, we plot $qP(q)L_w/\pi$ as a function of q. This representation emphasizes the differences between the fit and the experimental curves, when rodlike objects are studied. The experimental values of $qP(q)L_w/\pi$ are obtained from $M_w(R_\theta/Kc)_{c=0}$, and the theoretical curves are plotted using the theoretical form factor of a long, thin, rigid rod, with and without considering polydispersity in the rod length. The form factor of long, thin, rigid rods monodisperse in length is given by

$$P(q)_{\text{long}} = \frac{2}{qL}\int_0^{qL}\frac{\sin(qL)}{qL}\,\mathrm{d}(qL) - \left(\frac{2}{qL}\sin\left(\frac{qL}{2}\right)\right)^2 \quad (7)$$

To consider the influence of the size polydispersity on the scattering data, we considered a system of rods, polydisperse in length, with a Zimm−Schulz distribution.

$$w(L) = \frac{b^{z+1}}{z!}L^z\mathrm{e}^{-bL} \quad (8)$$

Here, $b = (z + 1)/L_w$ and z is the dispersion parameter ($z = 1/[(L_w/L_n) - 1]$). For micelles, monodisperse in length, z is infinite, while z decreases when the polydispersity increases. An important characteristic of the Holtzer−Casassa representation (Figure 4) is the presence of oscillations when the scattering particles are narrowdisperse in size; this oscillation is smoothed and disappears when the particle size polydispersity increases. The full black curve in Figure 4 represents the fit of the data to eq 7. The expression for monodisperse rods follows well the oscillation in the experimental data, which can still be observed for q larger than 10 μm^{-1}.

We have also tried to enhance the quality of the fit to the experimental data by considering the influence of rod flexibility by using the Koyama equation.[27] A reasonable fit cannot be obtained for a persistence length of $l_p < L_n$. This fit is shown in the Supporting Information.

To demonstrate the influence of both polydispersity and rod flexibility on the data analysis, we provide a second fit to the data as the upper gray curve in Figure 4. This curve has been arbitrarily shifted by 0.1 units for visual clarity. The fitting parameters are $z = 10$ (corresponding to $M_w/M_n = 1.1$) and $l_p = L_n$ (i.e., a rather stiff rod), and the radius of gyration deduced from this fit is $R_g \approx 280$ nm. One can see that, while the fitted line passes through the data points, it no longer follows the oscillation in the data. On the basis of this evidence, it appears that the structures present in solution have a rather narrow length distribution. Other fits are shown in the Supporting Information.

Dynamic Light Scattering (DLS) Experiments. When one studies rodlike structures by DLS, the scattered light is depolarized. The vertically polarized (VV) scattered light contains information about the translational and rotational modes, while the depolarized (VH) scattered light contains information about the rotational mode. Unfortunately, the depolarized data were too noisy to be analyzed; as a consequence, the results described here were obtained in the VV mode.

For monodisperse spherical structures, the electric field correlation function, $g^{(1)}(t_c)$, will exhibit simple exponential decay (eq 2). For rodlike structures in dilute solution, at large qL, additional exponential terms appear in the correlation function. These are due to local motion, particularly rotation and bending.[28,29] For data analyzed in terms of a cumulant expansion, the first cumulant, Γ_1, represents the mean relaxation rate of $g^{(1)}(t_c)$. Γ_1 increases as q^2 for purely translational motion and somewhat faster at high Γ_1 if rotational motion and bending become important.[30] Using the Maeda and Fujime expression for the apparent diffusion coefficient[31] (first cumulant), it is also possible to determine the principal diffusion coefficient of the structures.

$$\bar{\Gamma}/q^2 = (D_t + (L^2/12)D_r f_1(k) - (D_{||} - D_\perp)(^1/_3 - f_2(k))) \quad (9)$$

where $k = qL/2$, $D_{||}$ and $D_\perp$ are the coefficients for translation parallel and perpendicular to the rod's axis, D_r is the rotational diffusion coefficient, and D_t is the overall translational diffusion coefficient of the rod. The functions $f_1(k)$ and $(^1/_3 - f_2(k))$ are weighting factors depending only on k. The term $f_1(k)$ accounts for the contribution of rotation to Γ/q^2. The term $(^1/_3 - f_2(k))$ accounts for the contribution of translational anisotropy.

Table 1. Diffusion Coefficients Obtained from Broersma Equations

D_t (m^2 s^{-1})	2.01×10^{-12}
$D_{\|}$ (m^2 s^{-1})	2.62×10^{-12}
$D_\perp$ (m^2 s^{-1})	1.70×10^{-12}
D_r (s^{-1})	13

In the limit $q \rightarrow 0$, $f_1(k) \rightarrow 0$ and $f_2(k) \rightarrow {}^1/_3$. Therefore, the extrapolated value of Γ/q^2 to $q = 0$ gives the translational diffusion coefficient. The values of D_t, $D_{\|}$, $D_\perp$, and D_r can be calculated via Broersma equations[32−34] (Table 1).

A preliminary study has been carried out for the solution at $c = 0.33$ mg/mL.[35] The dependence of Γ/q^2 as a function of q^2 is shown in Figure 5. An acceptable fit of the experimental results given by eq 9 was obtained using a cross-sectional hydrodynamic diameter of 18 nm. According to this fit, $D_t = 2.01 \times 10^{-12}$ m^2/s and $D_r = 13$ s^{-1} (see Table 1 for all of the values). From the value of D_t, it is possible to deduce an apparent hydrodynamic radius at $c = 0.33$ g/mL, using the Stokes−Einstein relationship (eq 3). In this way, we calculate $R_{h,app} = 124$ nm, leading to $R_{g,app}/R_{h,app} = 2.3$ at this concentration. This ratio, larger than 2, agrees with the idea that the micelles in solution have a rodlike shape.

By CONTIN analysis, we should be able to distinguish the rotational diffusion coefficient at large angles. However, since D_r is small (13 s^{-1}), we do not expect to be able to separate its peak from the contribution of the translational diffusion coefficient at high angles. In Figure 6, we present a CONTIN plot, for three scattering angles, for a solution of PFS_{40}-*b*-$PDMS_{480}$ in decane at a concentration of 0.33 mg/mL. At each scattering angle, there are three components to the decay, a strong peak at a long relaxation time plus two weak peaks, with amplitudes less than 4% of that of the slow mode, at much shorter relaxation times. As we suspected, it is not possible to see a clear contribution of the rotational mode in the CONTIN plot.

Flexibility of the Micelles. Schmidt and Stockmayer[36] proposed a relationship between the diffusion coefficients of a rod and its Kuhn length, l_k:

$$\frac{D_{\|} - D_\perp}{D_t} = \frac{3}{4}\left[1 - 0.5\left(\frac{L}{l_k}\right)^{1/4}\right] \qquad (10)$$

From eq 10 and the data obtained at $c = 0.33$ mg/mL from Broersma equations (see Table 1), we calculate $l_k = 3.4$ μm. Since the Kuhn length is twice the persistence length, l_p, we can deduce that $l_p = 1.7$ μm, in agreement with the simulation performed on the static light scattering data. This value is close to but slightly larger than the micelle length determined from analysis of the SLS data, leading to the conclusion that the micelles are almost rigid on this length scale.

Using the Kuhn length value 3.8 μm obtained from the DLS study, one can give a more accurate value of the radius of gyration, which is modified due to the presence of a slight flexibility in the micelle. Benoît and Doty[37] derived an expression relating the persistence length to the radius of gyration for wormlike, or semiflexible, structures

$$\langle R_g^{\,2}\rangle = \frac{Ll_p}{3} - l_p^{\,2} + \frac{2l_p^{\,3}}{L} - 2l_p^{\,4}\frac{\left(1 - \exp\left(-\frac{L}{l_p}\right)\right)}{L^2} \qquad (11)$$

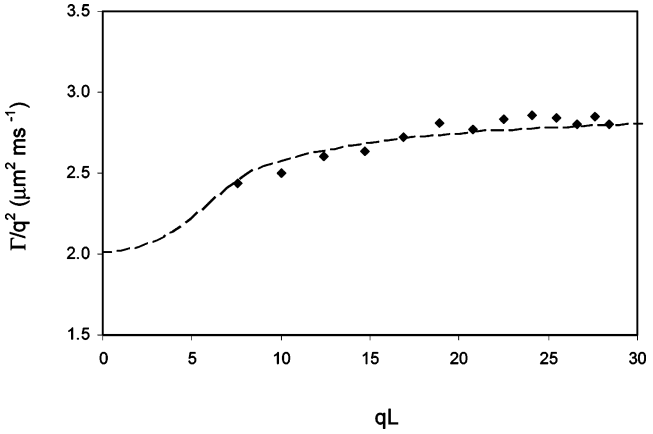

Figure 5. Γ/q^2 versus qL data (full diamonds) obtained at a polymer concentration of 0.33 mg/mL. The dashed curved is a fit of Γ using the Maeda equation (eq 9) with $L = 1050$ nm and $d = 18$ nm.

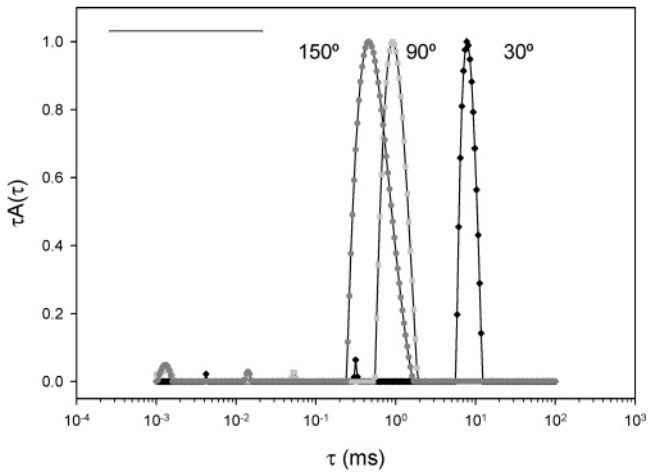

Figure 6. CONTIN plots for PFS_{40}-*b*-$PDMS_{480}$ assemblies in *n*-decane at 25 °C ($c = 0.33$ mg/mL) at scattering angles of 30, 90, and 150°.

From this equation, we calculate that the apparent radius of gyration of the micelle (at $c = 0.33$ mg/mL) is $R_{g,app} = 287$ nm. This has to be compared with the apparent radius of gyration deduced from the length of this structure at the same concentration ($c = 0.33$ mg/mL), where $L = 1050$ nm and $R_g = 303$ nm. There is a small decrease in the magnitude of the radius of gyration due to this slight flexibility, but this decrease does not significantly affect the magnitude of the ratio $R_{g,app}/R_{h,app}$, which remains larger than 2 (2.1).

Proposed Model of the Aggregation of the Micelles in Solution. Very few models can account for structures that are ~1 μm long, thin (cross-sectional hydrodynamic diameter 18 nm), and rigid and contain only 0.6 molecules/nm. One such model is shown in Figures 7 and 8. The structure in the figures is a ribbonlike monolayer of extended PFS chains that fold back upon themselves, with the PDMS corona chains protruding from the edge of the ribbon. In this model, the PFS chains have a zigzag structure corresponding to their structure in the crystalline homopolymer, with a 6.4 Å spacing between Fe atoms on adjacent chains. We draw the PFS chains as extended in the direction perpendicular to the long axis of the ribbon. The dashed line surrounding the structure depicted in Figure 7 represents the space occupied by the PDMS corona.

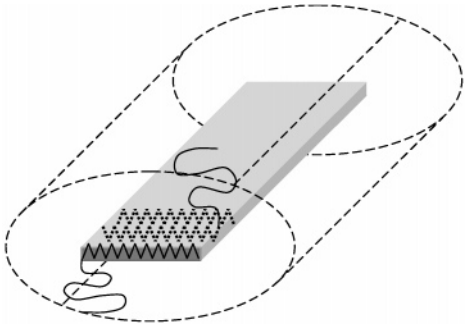

Figure 7. Proposed ribbonlike model of the assembly of the PDMS−PFS block copolymer in *n*-decane.

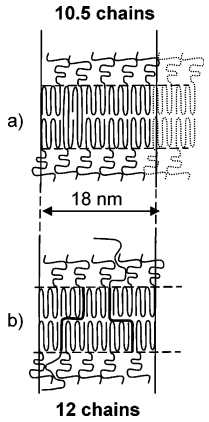

Figure 8. Top view of the structure presented in Figure 7. The folded chains represent the PFS block, which form the core of the structure, while PDMS chains form the corona: (a) with two possible types of PFS folding leading to the same linear aggregation number, $n = 0.6$ molecules/nm; (b) with the presence of two additional and incompletely folded chains (shown as darker lines) incorporated into the assembly, leading to $n = 0.67$ molecules/nm.

In Figure 8a, we suggest that PFS chains can fold so that two chains can span the width of the ribbon or that individual chains can reach across this width. This structure is drawn to accommodate the result of 10.5 chains per 18 nm of length. One of the surprising results from our experiments is the increase of the Holtzer plateau in Figure 2b, which suggests that the number of molecules per unit length increases with polymer concentration. One should recall that each sample was prepared separately at high temperature and then cooled to 25 °C. Thus, it is possible that, instead of indicating side-by-side association as the concentration increased, the plateau value may actually indicate somewhat different packing of PFS chains within the semicrystalline PFS domains. These differences might reflect a kinetic influence on, or concentration dependence of, the self-assembly process. We depict one such possibility in Figure 8b, in which we show two chains as heavier lines that have a different conformation within the ribbonlike structure with a greater number of segments in the amorphous region. In the drawing in Figure 8b, there are 12 chains per 18 nm of length. However, this slight difference in conformation increases the linear aggregation number from 0.60 in Figure 8a to 0.67 molecules/nm in Figure 8b.

We also considered structures in which the PFS chains were elongated parallel to the ribbon axis to form crystalline domains. In such a structure, the PDMS domains would protrude from the top and bottom faces of the ribbon. This type of structure has some analogy

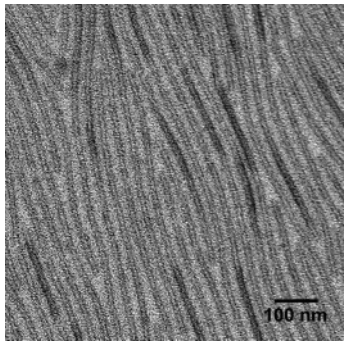

Figure 9. TEM micrograph of PFS_{40}-*b*-$PDMS_{480}$ assemblies prepared in *n*-decane at 60 °C, cooled to room temperature, and then allowed to age for 24 h. The sample was prepared by dipping a carbon-coated grid into the warm solution. The sample was not stained.

to the cylindrical self-assembled structures formed by the hairy rigid-rod polyelectrolytes studied by the Wegner group.[38] From our perspective, it is difficult to see why this type of packing would lead to ribbonlike structures instead of broader lamellae, and it is much more difficult for us to imagine what factors might limit the length of the elongated structures. The transverse folding depicted in Figure 8 accommodates the narrow molar mass and composition distribution of the PFS block copolymer, but it does not provide a compelling explanation for two of the most striking findings from the light scattering experiments: the apparent narrow length distribution and the substantial stiffness of the structures that are formed.

Comparison with the Structures in the TEM Images. In Figure 9, we present a typical TEM image obtained from a decane solution of these block copolymer assemblies. The images are not stained, and contrast comes from the electron-rich PFS component. One observes a monolayer of close-packed long objects that appear to be hollow. The samples were prepared by placing a drop of the decane solution on a carbon-coated grid, wicking away excess solvent with a piece of filter paper, and allowing the remaining solvent to evaporate at room temperature. We imagine that the flow fields associated with the wicking step brought the extended structures into contact. One can estimate the persistence length of the objects on the grid with the following expression:[39]

$$\langle \cos \varphi \rangle = \exp\left(-\frac{x}{2l_p}\right) \tag{12}$$

which is appropriate for structures confined to a two-dimensional space. In this expression, φ is defined as the angle between two tangents to a tube edge that delimit the arc length, x. From approximately 70 structures taken from seven images with one to two arc lengths per structure, we calculate that l_p is equal to $\sim 1\,\mu$m. The magnitude of l_p calculated for these samples is likely influenced by the neighboring structures in this two-dimensional nematic phase.[40]

What is most striking to us are the differences between the structures seen on the TEM grid and those inferred from the light scattering experiments in dilute solution. The "tubelike" structures seen in the TEM micrograph are much longer (tens of micrometers) and appear to be wider than those seen in solution. For example, individual objects seen in the TEM image appear to have a PFS core diameter of 20 nm, whereas

the DLS results suggest that the structures in dilute solution (0.33 mg/mL) are best characterized by a hydrodynamic diameter of 18 nm. The latter value includes the contribution of the PDMS corona. Thus, there appears to be a structural rearrangement or higher level of hierarchical self-assembly that takes place in concentrated solution as the solvent evaporates.

The nature of these changes remains a mystery. Among ourselves, we have often debated whether the objects seen in the TEM could be flattened or ribbonlike. For example, we observed by AFM that isolated rodlike micelles formed by $PFS_{40}-PI_{300}$ (PI = polyisoprene), when spin-coated onto a silicon wafer, were only 9 nm high, even though the dense PFS core seen in the unstained TEM image was 20 nm wide. On the other hand, we would expect ribbonlike structures to exhibit occasional twists. We have never seen twisted structures in TEM images of PFS−PDMS block copolymer micelles formed in alkane solvents.

Summary

Light scattering experiments (both static and dynamic) carried out on solutions of the diblock copolymer PFS_{40}-*b*-$PDMS_{480}$ in decane at 25 °C provide important insights into the properties of the self-assembled structures that are formed. A form-factor analysis of the static light scattering data indicates that the structures are long and thin and have the scattering properties of rigid rods. From the Holtzer−Casassa plateau, we infer that the rodlike micelles have a mean length of $L \approx 960$ nm and contain 0.6 molecules/nm. From both the static light scattering results and the cumulant analysis of the DLS results, we find that the self-assembled structures have an unexpectedly narrow distribution of sizes, with $M_w/M_n \approx 1.1$ and with only a small flexibility ($l_p \approx 1.7$ μm). From a cumulant analysis of the DLS results, we calculate that the hydrodynamic diameter of the micelles is ~18 nm. To account for the very small number of polymer molecules per unit length, we propose a thin ribbonlike structure for the species formed in dilute solution.

Remarkably, when solutions of these micelles are placed on a TEM grid and rapidly concentrated by blotting them with the edge of a filter paper and the remaining decane is allowed to evaporate, the structures observed are longer and appear to be wider and thicker than those present in dilute solution. It appears that the micelles themselves undergo a higher order self-assembly to form the tubelike structures seen in Figure 9, with lengths on the order of tens of micrometers and a persistence length of ~1 um. Many aspects of the self-assembly process for $PFS_{40}-PDMS_{480}$ in decane remain a mystery. The system is fascinating, but there clearly remains much work to be done.

Acknowledgment. The authors thank NSERC Canada for its support of this research. J.R. is grateful for an Ontario Graduate Scholarship. We thank Prof. Walther Burchard (University of Freiburg), Prof. Timothy Lodge (University of Minnesota), Prof. Matthias Ballauff (University of Bayreuth), and Dr. Christophe Chassenieux (Université Pierre et Marie Curie) for helpful discussions. We are also very much indebted to one of the reviewers for comments and suggestions.

Supporting Information Available: Koyama equation and figures showing plots of $qP(q)L_w/\pi$ as a function of q. This material is available free of charge via the Internet at http://pubs.acs.org.

Note Added after ASAP Publication. This article was released ASAP on August 13, 2005. The first sentence in the caption of Figure 5 has been revised. The correct version was posted on August 18, 2005.

References and Notes

(1) Massey, J.; Temple, K.; Cao, L.; Rharbi, Y.; Raez, J.; Winnik, M. A.; Manners, I. *J. Am. Chem. Soc.* **2000**, *122*, 11577.
(2) Massey, J.; Power, K. N.; Manners, I.; Winnik, M. A. *J. Am. Chem. Soc.* **1998**, *120*, 9533.
(3) Alexandridis, P.; Lindman, B. *Amphiphilic Block Copolymers*; Elsevier Science B. V.: Amsterdam, The Netherlands, 2000.
(4) (a) Tuzar, Z.; Kratochvil, P. *Adv. Colloid Interface Sci.* **1976**, *6*, 201. (b) Price, C. *Pure Appl. Chem.* **1983**, *55*, 1563. (c) Xu, R.; Winnik, M. A.; Hallett, F. R.; Riess, G.; Croucher, M. D. *Macromolecules* **1991**, *24*, 87. (d) Zhu, J.; Eisenberg, A.; Lennox, R. B. *J. Am. Chem. Soc.* **1991**, *113*, 5583.
(5) (a) Papkov, V. S.; Gerasimov, M. V.; Dubovik, I. I.; Sharma, S.; Dementiev, V. V.; Pannell, K. H. *Macromolecules* **2000**, *33*, 7107. (b) Chen, Z.; Foster, M. D.; Zhou, W.; Fong, H.; Reneker, D. H.; Resendes, R.; Manners, I. *Macromolecules* **2001**, *34*, 6156.
(6) (a) Lotz, B.; Kovacs, A. J. *Kolloid Z. Z. Polym.* **1966**, *209*, 97. (b) Kawai, T.; Shiozaki, S.; Sonoda, S.; Nakagawa, H.; Matsumoto, T.; Maeda, H. *Makromol. Chem.* **1969**, *128*, 252. (c) Dröscher, M.; Smith, T. L. *Macromolecules* **1982**, *15*, 442. (d) Richter, D.; Schneiders, D.; Monkenbusch, M.; Willner, L.; Fetters, L. J.; Huang, J. S.; Lin, M.; Mortensen, K.; Fargo, B. *Macromolecules* **1997**, *30*, 1053. (e) Lin, E.; Gast, A. *Macromolecules* **1996**, *29*, 4432.
(7) Vilgis, T.; Halperin, A. *Macromolecules* **1991**, *24*, 2090.
(8) Cao, L.; Manners, I.; Winnik, M. A. *Macromolecules* **2002**, *35*, 8258−8260.
(9) Raez, J.; Manners, I.; Winnik, M. A. *J. Am. Chem. Soc*. **2002**, *124*, 10381.
(10) Raez, J.; Manners, I.; Winnik, M. A. *Langmuir* **2002**, *18*, 7229.
(11) Raez, J.; Tomba, J. P.; Manners, I.; Winnik, M. A. *J. Am. Chem. Soc*. **2003**, *125*, 9546.
(12) Raez, J. A study of organometallic block copolymer "nanobarrels" using electron microscopy and scattering techniques. Ph.D. Thesis, University of Toronto, Toronto, ON, Canada, 2004.
(13) Massey, J. A.; Kulbaba, K.; Winnik, M. A.; Manners, I. *J. Polym. Sci., Polym. Phys.* **2000**, *38*, 3032.
(14) Schillen, K.; Yekta, A.; Ni, S.; Farinha, J. P. S.; Winnik, M. A. *J. Phys. Chem. B* **1999**, *103*, 9090.
(15) Yaws, Carl L. *Chemical Properties Handbook: Physical, Thermodynamic, Safety, and Health Related Properties for Organic and Inorganic Chemicals*; McGraw-Hill: Toronto, Canada, 1999; p 495.
(16) Siegert, A. J. F. Massachusetts Institute of Technology, Rad. Lab Rep No. 465, 1943.
(17) (a) Provencher, S. W. *J. Chem. Phys.* **1976**, *64*, 2772. (b) Provencher, S. W. *Comput. Phys. Commun.* **1982**, *27*, 213. (c) Provencher, S. W. *Comput. Phys. Commun.* **1982**, *27*, 229.
(18) Koppel, D. E. *J. Chem. Phys.* **1972**, *57*, 4814.
(19) Benoît, H.; Froelich D. Application of Light Scattering to Copolymers. In *Light Scattering from Polymer Solutions*; Huglin, M. B., Ed.; Academic: London, 1972; Chapter 11.
(20) Tsunashima, Y.; Suzuki, S. *J. Phys. Chem. B* **1999**, *103*, 8675.
(21) This value is in agreement with the value (−0.010 mL/g, λ_0 = 633 nm) reported in Soria, V.; Llopis, A.; Celda, B.; Campos, A.; Figueruelo, J. E. *Polym. Bull.* **1985**, *13*, 83.
(22) Bushuk, W.; Benoît, H. *Can. J. Chem.* **1958**, *36*, 1616.
(23) Tsunashima, Y.; Kawamata, Y. *Macromolecules* **1993**, *26*, 4899.
(24) Brown, W. *Light Scattering: Principles and Development*; Clarendon Press: Oxford, U.K., 1993.
(25) Hammers, W. E.; Ligny, C. L. *J. Polym. Sci., Polym. Phys. Ed.* **1974**, *12*, 2065.
(26) Holtzer, A. *J. Polym. Sci.* 1955, *17*, 432.
(27) Koyama, R. *Phys. Soc. Jpn.* **1973**, *34*, 1029.
(28) Tracy, M. A.; Pecora, R. *Annu. Rev. Phys. Chem.* **1992**, *43*, 525.
(29) (a) Tracy, M. A.; Pecora, R. *Macromolecules* **1992**, *25*, 337. (b) Phalakornkul, J. K.; Gast, A. P.; Pecora, R. *Macromolecules* **1999**, *32*, 3122.

(30) Nicolai, T.; Mandel, M. *Macromolecules* **1989**, *22*, 2348.
(31) Maeda, T.; Fujime, S. *Macromolecules* **1984**, *17*, 1157.
(32) Broersma, S. *J. Chem. Phys.* **1960**, *32*, 1626.
(33) Broersma, S. *J. Chem. Phys.* **1960**, *32*, 1632.
(34) Broersma, S. *J. Chem. Phys.* **1981**, *74*, 6989.
(35) Since the structures appear to be rather rigid ($l_p > L_n$) and these are preliminary experiments, we restrict our data analysis to the case of rigid rods.
(36) Schmidt, M.; Stockmayer, W. H. *Macromolecules* **1984**, *17*, 509.
(37) Benoît, H.; Doty, P. *J. Phys. Chem.* **1953**, *57*, 958.
(38) Rulkens, R.; Wegner, G. and Thurn-Albrecht, T. *Langmuir* **1999**, *15*, 4022.
(39) (a) Landau, L. D.; Lifshitz, E. M. *Statistical Physics*, 3rd ed.; Pergamon Press: Oxford, U.K., 1980; p 399. (b) Frontali, C.; Dore, E.; Ferrauto, A.; Gratton, E.; Bettini, A.; Porzzan, M. R.; Valdevit, E. *Biopolymers* **1979**, *18*, 1353.
(40) (a) Dogic, Z.; Zhang, J.; Lau, A. W. C.; Aranda-Espinoza, H.; Dalhaimer, P.; Discher, D. E.; Janmey, P. A.; Kamien, R. D.; Lubensky, T. C.; Yodh, A. G. *Phys. Rev. Lett.* **2004**, *92*, 125503. (b) Dogic, Z.; Zhang, J.; Lau, A. W. C.; Aranda-Espinoza, H.; Dalhaimer, P.; Discher, D. E.; Janmey, P. A.; Kamien, R. D.; Lubensky, T. C.; Yodh, A. G. *Phys. Rev. Lett.* **2004**, *93*, 219902.

MA0498870